APPLICATION OF FISH SHOAL OPTIMIZATION: RESULTS AND DISCUSSION

The actual problem of riprap riveted earthen channel design has 5D Euclidean search space and it was solved by pre-assigning a particular type of riprap stone for the channel design. Since the fish shoal optimization algorithm can handle all types of riprap stones in its single computational program, therefore, the objective function of the problem turned out to be a 6D problem. The additional sixth dimension was meant to characterize the type of riprap stone which fish shoal optimization algorithm will search to identify the best type of riprap stone for revetment purpose. Therefore, the model for the actual problem needs was revised to suit the characteristic of fish shoal optimization method. The revised model, its dimensionless form, application procedure for fish shoal optimization algorithm, results and discussions, and conclusions drawn out of the comparison of performances of fish shoal optimization algorithm with published data and results of particle swarm optimization method are described in the following subsections.

7.1 The Model

In order to determine the cross sectional dimensions of a minimum cost earthen trapezoidal canal having side slopes lined with loose riprap stones and unlined bottom, the size of riprap stones, and the most suitable type of stones, the objective function (*Cost,* \$/m) was formulated as:

Minimize $Cost(b, m_1, m_2, y, D, \phi) = c_1 A_t + (c_{2.1} P_s || c_{2.2} P_s || c_{2.3} P_s) + c_3 T$ (7.1) where

$$A_{t} = b(y+f) + (m_{1}+m_{2})\frac{(y+f)^{2}}{2}$$
(7.2)

$$P_{s} = \left[\left(\sqrt{1 + m_{1}^{2}} + \sqrt{1 + m_{2}^{2}} \right) (y + f) \right]$$
(7.3)

$$T = b + (y + f)(m_1 + m_2)$$
(7.4)

 c_1 , $c_{2.1}$, $c_{2.2}$, $c_{2.3}$, and c_3 are the cost of earth excavation per unit volume (\$/m³), costs of three types of riprap stones (\$/m²), and the land acquisition cost (\$/m²) per unit length of the canal, respectively. Symbol (||) represents 'or' logical operation. A_t , P_s , and T denote the total excavated area, wetted perimeter corresponding to the side slopes, and top width of the canal, respectively, including freeboard. It may be noted that the objective function (Eq. 7.1) is now having 6D search space.

7.1.1 Constraints

The non-linear minimization objective function for the least cost of canal is subjected to the constraints on flow rate, and shear stresses acting on stable riprap stones laid on the canal side slopes as:

$$\frac{Q}{k_n\sqrt{s_o}} - \left[\frac{[by]^{5/3}}{n_b b^{2/3}} + \frac{[m_1 y^2]^{5/3}}{2^{5/3} n_s [y\sqrt{1+m_1^2}]^{2/3}} + \frac{[m_2 y^2]^{5/3}}{2^{5/3} n_s [y\sqrt{1+m_2^2}]^{2/3}}\right] = 0(7.5)$$

$$N_s (G-1)\rho g D \sqrt{1 - \frac{k_{\phi}}{1+m_1^2}} - f_s \tau_s = 0$$
(7.6)

$$N_{s}(G-1)\rho g D \sqrt{1 - \frac{k_{\phi}}{1 + m_{2}^{2}}} - f_{s}\tau_{s} = 0$$
(7.7)

7.2. Dimensionless Problem Statement

The non-linear optimization problem was transformed to a dimensionless form. A repeating variable λ in terms of the problem associated parameters were defined in chapter 3 and the same was applied for non-dimensionalizing purpose as:

$$\lambda = \left(\frac{Q^2}{gS_o}\right)^{1/5} \tag{7.8}$$

The involved physical variables were transformed dimensionless as:

$$b_{*} = b/\lambda; D_{*} = D/\lambda; f_{*} = f/\lambda; y_{*} = y/\lambda$$

$$A_{t^{*}} = b_{*}(y_{*} + f_{*}) + (m_{1} + m_{2})\frac{(y_{*} + f_{*})^{2}}{2}$$
(7.9)

$$P_{s^*} = \left[\left(\sqrt{1 + m_1^2} + \sqrt{1 + m_2^2} \right) (y_* + f_*) \right]$$
(7.10)

$$T_* = b_* + (y_* + f_*)(m_1 + m_2)$$
(7.11)

The combination of cost of earth excavation (c_1) and non-dimensionalizing parameter (λ) were applied to transform the cost (per unit length) function of the canal in dimensionless form as:

$$C_* = \frac{Cost}{c_1 \lambda^2}; \ c_{2.1^*} = \frac{c_{2.1}}{c_1 \lambda}; \ c_{2.2^*} = \frac{c_{2.2}}{c_1 \lambda}; \ c_{2.3^*} = \frac{c_{2.3}}{c_1 \lambda}; \ c_{3^*} = \frac{c_3}{c_1 \lambda}$$
(7.12)

Manning's roughness coefficients were non-dimensionalized as:

$$n_{s*} = \frac{n_s \sqrt{g}}{k_n \lambda^{1/6}} = k_D D_*^{1/6} \text{ and } n_{b*} = \frac{n_b \sqrt{g}}{k_n \lambda^{1/6}}$$
 (7.13)

The use of dimensionless Manning's roughness coefficient (Eq. 7.13) in Eq.

7.5 yielded:

$$1 = \left[\frac{(b_* y_*)^{5/3}}{n_{b*} b_*^{2/3}} + \frac{(m_1 y_*^{2})^{5/3}}{2^{5/3} k_D D_*^{1/6} (y_* \sqrt{1 + m_1^2})^{2/3}} + \frac{(m_2 y_*^{2})^{5/3}}{2^{5/3} k_D D_*^{1/6} (y_* \sqrt{1 + m_2^2})^{2/3}}\right] (7.14)$$

Hence, the dimensionless problem statement formulated using Eqs. 7.1, 7.5-

- 7.7 took on the following form:
- $\begin{aligned} \text{Minimize } C_*(b_*, z_1, z_2, y_*, D_*, \phi) &= A_{t^*} + (c_{2.1^*} P_{s^*} \parallel c_{2.2^*} P_{s^*} \parallel c_{2.3^*} P_{s^*}) + c_{3^*} T_*(7.15) \\ \Psi_1(b_*, y_*, z_1, z_2, D_*) &= 1 F = 0 \end{aligned}$ (7.16)

where
$$F = \left[\frac{(b_* y_*)^{5/3}}{n_{b*} b_*^{2/3}} + \frac{(m_1 y_*^2)^{5/3}}{2^{5/3} k_D D_*^{1/6} (y_* \sqrt{1 + m_1^2})^{2/3}} + \frac{(m_2 y_*^2)^{5/3}}{2^{5/3} k_D D_*^{1/6} (y_* \sqrt{1 + m_2^2})^{2/3}}\right]$$

 $\Psi_2(b_*, y_*, z_1, z_2, D_*, \phi) = k_{xx} y_* - X D_* \sqrt{1 - \frac{k_{\phi}}{1 + m_1^2}} = 0$ (7.17)

$$\Psi_{3}(b_{*}, y_{*}, z_{1}, z_{2}, D_{*}, \phi) = k_{x}y_{*} - XD_{*}\sqrt{1 - \frac{k_{\phi}}{1 + m_{2}^{2}}} = 0$$
(7.18)

where $X = \frac{N_s(G-1)}{f_s S_o}$ is a dimensionless critical side slope shear-stress

coefficient (Froehlich 2011a). The non-dimensionalization translates the problem independent of units and scales down the actual Euclidean space into

a virtually squeezed down search space that makes the search operation easier and more efficient. However, Jain et al. (2004) and Reddy and Adarsh (2011) applied dimensionless cost coefficients in their objective functions for the design of minimum cost lined canals.

7.3 Application of Fish Shoal Optimization

An augmented cost function transformed the constrained minimization problem into an unconstrained problem as:

Minimize
$$AF = C_* + \sum_{j=1}^{3} \beta_j |R_j|$$
 (7.19)

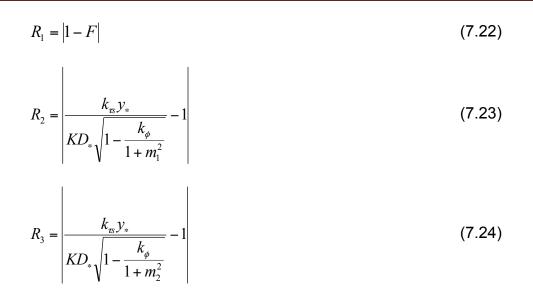
where *j* (=1, 2, and 3) refers to constraint Eqs. 7.16, 7.17, and 7.18, respectively. The penalty parameter β_j was defined as:

$$\beta_{j} = \begin{cases} 0 & \text{if } R_{j} \le \varepsilon \\ \eta & \text{if } R_{j} > \varepsilon \end{cases}$$
(7.20)

A tolerance limit (ε) was set as 10⁻⁶ for the violation of flow rate and shear stress constraint equations. To ensure a sufficient exploration of search space at initial stage with enhanced efficiency at later stage, a sequentially increasing penalty function (η) is:

$$\eta = a + \tanh\left(\frac{N_t}{N_{t\max}}\right) \quad for \ \forall \ j \tag{7.21}$$

The value of constant 'a' is in Table 7.1. Eqs. 7.16, 7.17 and 7.18, respectively, yielded residuals R_1 , R_2 and R_3 that arise out of violation of constraint equations as:



These residuals, multiplied with penalty parameters, were added to the objective function (Eq. 7.15) to get an augmented cost function for Fish Shoal Optimization to evaluate the performance of each shoal member.

7.3.1 Flow chart and creation of subgroups

Figure 7.1 shows the flow chart for Fish Shoal Optimization application. For accommodating three types of riprap stones, i.e., rounded, subrounded and subangular, and angular, range of the sixth dimension place [0, 1] is divided into three class-intervals, i.e., [0, 0.33],]0.33, 0.67], and]0.67, 1]. Lower limits for the second and third subgroups are '>0.33' and '>0.67', therefore their lower limits are shown as open-ended bracket ']'. Thus, fish shoal optimization algorithm invoked all kinds of riprap stones to create a population that mimics the social character of a fish shoal. The flow chart reveals that the shoal character sustained at all stages of optimization process

and it required one program code to choose the best riprap stone for the minimum cost design of earthen canal. Each solution array gave the size specifications of a canal and riprap stone, and the type of riprap stone as well.

7.3.2 Parameter setting

The shoal comprised three types of riprap (fish stones species/subgroups), therefore, the search space expected to engross three different promising zones of optimality. In order to facilitate global leader to emerge out from any subgroup, fish shoal optimization algorithm was initialized with a somewhat balanced value of the cognitive parameter (c_1 =1.957), i.e., approximately half (1.957) of the sum of cognitive and social parameter values (4.1). Based on the character (type of riprap stone) of global leader (which may change in successive generations), the shoal is driven in varying directions according to the number of promising zones. This facilitated an effective exploration of the search space. The value of ψ is 4.1 as per the suggestion of Clerc and Kennedy (2002) and the inertia weight was varied linearly in the range of [1, 0]. The maximum number of iterations (300) was the convergence criterion.

To avoid singularity or overshoot, a limit [10⁻⁵, 1] was imposed on the range of random numbers. Size of the shoal was 60 to accommodate approximately 20 solutions in each subgroup at the initial stage. The random number generator was initialized with the default setting of the HP ProBook 4510s laptop.

7.3.3 Range of variables

Based on the preliminary results, the range of canal width was set as 2.5 to15 m. The flow depth was in the range of [0.5, 5.0] in conformance with Gupta and Singh (2012) suggestion. Lower limits for the side slopes were set on the basis of real values (not imaginary) obtained from Eqs. 3.19-3.20. Since rounded stones are perceived desirable by the designers, therefore, the upper limit for the side slopes was set to be 3.0 than 2.5 recommended by Blackler and Guo (2009) to facilitate a relatively more conducive environment for the rounded stone to prove its superiority. The range of riprap stone size was set in a commercially viable interval of 0.1 to 1.0 m. A summary of the range of variables applied for solving the problem is in Table 7.2.

7.3.4 Manning's roughness coefficients for canal bottom

Unknown variables (Froude and Reynolds numbers) involved in Eq. 3.35 were determined by considering the canal to be an earthen canal without any riprap revetment with bed sediment size 1 mm. The canal cross-sectional features (area and perimeter) were determined using randomly generated solutions and Froude number was calculated. Manning's roughness coefficient for canal bottom (n_b) was determined by applying value of the Froude number. The actual flow rate through the canal whose sides were riveted with loose riprap and bottom was unlined was calculated using Eq. 3.17. The supercritical flow characteristic in earthen canal is not acceptable, therefore, a constant value of $n_b = 0.025$ (Froehlich 2011a) was set to fulfill the requirement of the

"if-else" loop of the program for Froude number value above 2, however, Table 7.3 shows that this condition never arose during computational run.

7.3.5 Cost calculation

Randomly generated initial solutions provided the trial mean-sizes of riprap stones (*D*) and the thickness of riprap layer on the side slopes was chosen to be 1.5 times the *D* (NCHRP Rep. 568, p. C4). The cost of riprap in $\$/m^3$ (round: 41; subround and subangular: 36.6; and angular stone: 31.4 $\$/m^3$) was multiplied by the riprap layer thickness (1.5 times the mean size) to determine the cost of riprap stones per square meter of coverage area ($\$/m^2$). The cost calculated in terms of $\$/m^2$ was applied in Eq. 7.15. These costs were updated during the computational process according to the updated sizes of riprap stones. Realistic data for average costs of earth excavation (4.052 $\$/m^3$) and land acquisition (2.84 $\$/m^2$) were obtained from an Arizona (USA) canal project under U.S. Bureau of Reclamation.

7.4 Results and Discussion

The published problem of Froehlich (2011a) was adopted to validate the proposed optimization algorithm.

7.4.1 Shoal convergence characteristic

Figure 7.2 shows the characteristic of shoal population during flow rate convergence. The presence of three markers (red , blue+, green×) at all stages with varying markers' concentration along the x-axis reveals the existence of members from all three subgroups with increasing population of

Chapter 7

dominating subgroup members (subround and subangular, and angular riprap stones) that may result in the minimum cost canal. Rounded stone dominated the initial shoal, whereas the angular stone subgroup finds prominence in converged shoal (see Figure 7.2). It further reveals that the fish shoal, while maneuvering towards the global minimum, encounters various local sub-optimal zones, and hence acclimatizes its character to fit with the en route local environment. Therefore, the majority of the shoal members maneuver towards the subgroup to which global leader associates. Thus, changes in the concentration of members from different subgroups occur with successive iterations (see Figure 7.2).

Figure 7.3 displays the convergence characteristics of local best cost, mean shoal cost, and the global minimum cost members obtained so far with iterations for three freeboard scenarios. Involvement of members from different subgroups with significant cost difference did not allow the mean shoal cost at initial iterations to converge until the computational run crosses about 230 iterations (see Figure 7.3). Another reason for this feature is associated with the incremental increase in the penalty parameters' values with iteration numbers that forces the mean shoal cost to rise up initially due to the presence of larger residuals. However, the initial non-converging characteristic helps in maintaining sufficient heterogeneity in the shoal population that spreads across the spectrum of different subgroups. The population heterogeneity builds up additional pressure on shoal members to perform their best to locate

the global optima. The occurrence of convergence of the mean shoal cost curve close to the end of iterations (see Figure 7.3) reflects a relatively more homogeneous population dominated by specific subgroup members. Thus, the shoal population tends to become less heterogeneous by eliminating the poorly performing subgroup members (see Figure 7.2). Further, the significant cost variation between the members of different subgroups did not allow mean shoal cost to converge with the global minimum curve as the shoal maintains heterogeneity even after the end of iterations.

7.4.2 Changing global leader and operational philosophy

The varying subgroup of global leader with iterations is shown in Figure 7.4. Red, pink, and green color markers (, + and ×) represent global leader from rounded, subround-and-subangular, and angular riprap subgroups, respectively. Based on the local best cost and cost of global leader, global leader and/or its associated subgroup may or may not change with iterations (see Figure 7.4). The emerging global leader (say, angular stone subgroup) causes other subgroup (rounded and subround-and-subangular) members to go in minority (see iterations 250 to 300 in Figure 7.2) and attempts to make them extinct during subsequent iterations, if it continues to drive the shoal movement. However, successive iterations may produce a new global leader from other subgroup (see Figure 7.4) that may cause the shoal character to change as per its personal subgroup, thus, a new breed of shoal population comes up in majority. The emergence of global leader from subround-and-

subangular riprap subgroup during the middle of iterations (see pink symbol + in Figure 7.4) and its effect on shoal character is evident from the increased concentration of blue color marker (+) in Figure 7.2.

Similar to its ancestor, fish shoal optimization also persuades the shoal to track the movement of global leader emerging out from any subgroup. A stiff competition between the members from the subgroup of global leader and the shoal members from other subgroups always prevails. The global leader acts as a monarch that forces the other subgroup members to go into extinction, and this condition compels the members from other subgroups to perform their best to acquire the position of leader for the survival of their community/subgroup. Thus, fish shoal optimization promotes the population outburst of the fittest subgroup members in tune with Genetic Algorithms that works on the premise of survival of the fittest. This way, fish shoal optimization acquires a unified strength of Genetic Algorithms and Particle Swarm Optimization techniques.

7.4.3 Global leader's characteristic for flow rate convergence

Figure 7.5 shows the changing character (subgroup) of global leader during convergence process of flow rate with iterations for three freeboard scenarios to avoid confusion arising out of the overlap of different curves. The initial search spread over the range of 0-125 m³/s with rounded and subround and subangular riprap which eventually narrowed down to the target of 60 m³/s flow rate at the end of iterations. Earlier convergence of '*f* = 0' scenario curve

Chapter 7

relative to f = 0.5 and $f = 0.5y^{0.25}$ in sequence reveals that the inclusion of an additional freeboard parameter delays the convergence because of the shift of promising zone and/or extension of the search space. The varying subgroup of global leader with iterations portrays the capability of fish shoal optimization to accommodate three types of riprap stones at all stages of iterations to choose the most suitable type of riprap stone that yields the minimum cost. The change in subgroup of global leader with iterations may not necessarily be in sequence from round to subround-and-subangular to angular, and a member from any subgroup can emerge out as global leader to drive the movement of shoal towards global minimum. Thus, a thorough exploration of the search space with varying direction of shoal maneuver occurring due to changing of global leader ensured a stiff competition among the members from different subgroups. The successive iterations generated more members from better subgroup (angular riprap) for competition which is similar to a characteristic of Genetic Algorithms where fittest members are picked up for crossover operation in successive iterations to generate better off springs for stiff competition.

7.4.4 Global leader's characteristic for shear stress convergence

Figures 7.6 (a) and (b) show the convergence characteristic of the global leader emerging out from different subgroups during the iterative process for shear stress residual convergence obtained from the calculation of left hand side (LHS) of Eqs. 7.6 and 7.7, respectively. The convergence

characteristic for only three freeboard scenarios [f = 0 (blue line), 0.5 (black line) and $0.5y^{0.25}$ (red line)] are meant to avoid the confusion arising out of the excessive overlap of curves and/or points. The changing subgroup of global leader ensured a healthy competition among different subgroup members. It also confirmed that the parameter settings of fish shoal optimization with sequentially increasing penalty functions are effective to diminish the shear stress residuals to zero (see Figure 7.6). Positive magnitude of shear stress residuals obtained for global leader at all iterations implies that the exploration of Euclidean search space occurred where riprap stones remain stable. Hence, almost all points lie above the x-axis.

7.4.5 Shoal characteristic at the end of iterations

The characteristics of converged shoal- cost of canal, summation of residuals ($R_1+R_2+R_3$), and type of stones, at the end of iterations are shown in Figures 7.7-7.11 for five different freeboard scenarios. The x-, y-, and z- axis represent the type of riprap stones, cost of construction and the sum of residuals, respectively. Figures 7.7 and 7.9-7.11 reveal that the better performing subgroups of riprap stones (subround-and-subangular and angular stones) that remain alive and they forced round stone subgroup to go into extinction. The converged shoal comprised the largest population of angular stone subgroup than other types and they yielded the minimum cost canal (see red points '*' relating to angular stones on the x-y plane in Figures 7.7-7.11). Members of the shoal display a varying degree of constraint violation with

decreasing magnitude of summation of residuals ($R_1+R_2+R_3$) that result in cost reduction. Figure 7.8, drawn for f = 0.5, shows the shoal after 300 iterations comprised all types of riprap stones with smallest population size of round stone subgroup and the largest subgroup of angular stone that has relatively the lowest cost. The subround and subangular riprap stands next to the angular stone with a relatively higher cost and different canal dimension. The round riprap stone stands the last for giving the costliest canal.

7.4.6 Impact of freeboard scenarios on fish shoal optimization algorithm performance

Comparison of the results involving two different parameter settings (see Table 7.1) revealed that fish shoal optimization could not yield good results for the depth dependent freeboard scenarios ($f = 0.5y^{0.25}$, $0.25+y^{0.25}$, and $0.25+y^{0.5}$) with parameter setting-1 but better results were obtained for the first two freeboard scenarios. Parameter setting-2 for fish shoal optimization gave better results for the three depth dependent freeboard scenarios but it trapped into local sub-optimal zone comprised by the subround and subangular stone for f = 0 scenario. It shows that a different set of penalty functions for each freeboard scenario should be applied instead of applying a single set of penalty functions for all scenarios, and it seems logical. Thus, results for the initial two sets of freeboard scenarios were taken up from the

parameter setting 1 and the other three were adopted from the parameter setting 2 for analysis purpose.

7.4.7 Selection criteria for the global leader and results

Table 7.3 presents a pair of solutions for each freeboard scenario. These solutions were selected based on the global minimum cost and the lowest sum of all residuals. These solutions emerging out from only angular stone subgroup do not differ significantly from each other and the costs of construction are almost the same. The same size of stones applied for the revetment of either side of a canal caused fish shoal optimization to yield the zero/negligible shear stress residuals, hence all solutions (see columns 6-7) provided symmetric cross sections to yield minimum cost canal. The reason of the best performance of angular riprap stone lies in its ability to remain stable on the steeper side slopes because of higher mass angle of repose (Gupta and Singh 2012) and interlocking capability that further enhances stability on steeper slopes similar to what it does in road pavements. They afford to sustain even more shear stresses than that induced by the flowing water. This finding is in conformity with the findings of Gupta and Singh (2012) and Gupta et al. (2014). The steeper side slope decreased the top width, hence land acquisition cost. The scope of sustaining higher shear stresses by angular riprap stones allowed fish shoal optimization to proceed for acquiring higher flow velocity, which, in turn, squeezes the cross sectional area to reduce the excavation cost as well. Additional benefit arises from the reduction in the cost of clearing, grubbing, moving and relocation activities required over reduced land width/right of way. The lesser requirements of earth excavation, land area, and clearing, grubbing, moving and relocation activities reduce the construction time significantly. Thus, the type of riprap stone used for lining the canal side slopes also plays a vital role to affect the cost, performance, and time of completion of the canal construction project.

7.4.7.1 Canals with and without freeboard

Comparison of canal configurations for f = 0 and 0.5 shows that the canal with fixed magnitude of freeboard (0.5m) possesses a larger bottom width (7.9272 m), top width (17.9463 m) and side slope length (12.1988 m), lower flow depth (2.9795 m) and excavated area (36.3999 m²), steeper side slopes (1.4398), higher flow velocity (1.6479 m/s), and a relatively larger cost (293.0276 \$/m) as compared to that having no freeboard (compare initial two rows in Table 3 for parameter setting-1). Fish shoal optimization reduced the length of canal sidewalls and top width by acquiring steeper side slopes and reduced flow area to accommodate the required flow rate (compare data in column 12 of the first two rows in Table 7.3). Provision of freeboard with canal section resulted in both the increased top width and length of sidewalls but the finding of squeezed cross section area conforms to the findings of Guo and Hughes (1984) for hydraulically most efficient channel. Table 7.3 (compare the

first scenario with the remaing four) further illustrates that the cost of canal without freeboard provision is lower than that with freeboard.

7.4.7.2 Effect of land area cost in objective function

The relatively reduced flow areas achieved by the canals riveted with angular riprap stones permitted higher flow velocities, which in turn, made them hydraulically efficient. The inclusion of top width (land area) with flow area and perimeter in objective function yielded not only the cost effective but also a most hydraulically efficient canal section. The involvement of three canal features in minimization process put an additional pressure on fish shoal optimization to minimize the magnitudes of involved physical variables *b*, m_1 , m_2 , and *y* for the minimum cost canal. The costs associated with the excavated area, perimeter and top width can be viewed as a weighting factor applied to the three terms, and thus, the objective function serves as a unified expression for both the maximization of hydraulic efficiency and the minimization of cost.

7.4.7.3 Depth dependent versus fixed magnitude freeboard scenario

An intra-comparison of the results for three depth dependent freeboard scenarios given in Table 7.3 (parameter setting 2) shows that the bottom widths, flow depths, side slopes, and flow velocities are marginally different for them, hence their cost. Thus, it can be inferred that the most optimal zone for depth dependent freeboard scenarios remains closer in Euclidean search

space and it shifts away for other two freeboard (f = 0 and 0.5m) scenarios independent of flow depth (see significantly different values of *b*, *y*, m_1 and m_2). Therefore, freeboard scenarios affected the search process and optimal canal configurations that raised a need of two different parameter settings for depth dependent and independent freeboard scenarios.

7.4.7.4 Comparison of the results with earlier published works

The present results obtained for the minimum cost canals without freeboard (A_f = 36.8223 m², P_f = 17.9108 m, D = 0.1029 m) are found far superior to that obtained by Gupta and Singh (2012) for the most hydraulically efficient canal applying area minimization (A_f = 47.2621 m², P_f = 19.9496 m, D = 0.1182 m) and perimeter minimization (A_f = 45.7289 m², P_f = 20.2965 m, D = 0.0940 m) separately (refer to solution numbers 11-12 in their Tables 7.1-7.2). Further, construction costs of hydraulically most efficient canal obtained by Froehlich (2011a) are calculated as 295.9 and 303.6 \$/m for angular and subround-and-subangular stones revetment, respectively. It is important to note that the cost obtained by fish shoal optimization for the canal without freeboard (253.6108 \$/m) comes out to be 14.29 and 16.47% less than that of Froehlich (2011a) canal having angular and subround and subangular stones revetment, respectively.

7.5 Comparison of Results with Those Obtained by Particle Swarm Optimization

It is evident from the results of particle swarm optimization method that the sediment-laden flow condition near channel bottom yield lower cost of construction, therefore, sediment-laden flow condition was applied for the application of fish shoal optimization algorithm. Since the fish shoal optimization algorithm resulted in solutions relating to the angular stone revetment, therefore, angular stone revetment cases from the application of particle swarm optimization can only be compared. Table 7.3 (Parameter setting1, column 15, rows 1-4) reveals that the cost of channel construction for the freeboard scenarios f = 0 and f = 0.5 are 253.6108 and 293.0299\$. respectively. These costs are less than those obtained (256.9989, 308.1187 \$) by the application of particle swarm optimization method (see Table 5.5, Case II, column 15, rows 1-2) for the freeboard scenarios f=0 and f=0.5, respectively. Similarly, the costs of channels obtained by fish shoal optimization algorithm for other freeboard scenarios ($f = 0.5 v^{0.25}$, f = 0.25+ $0.25 y^{0.25}$, $f = 0.25 + 0.25 y^{0.5}$) are 310.0780, 302.6389 and 312.5735\$, respectively. However, the application of particle swarm optimization method yielded cost of channels as 324.4233, 316.1790, and 326.9636\$, respectively for the other freeboard scenarios $f = 0.5 y^{0.25}$, $f = 0.25 + 0.25 y^{0.25}$, and f = 0.25+ 0.25 $v^{0.5}$. Therefore, it can be inferred that the application of fish shoal optimization algorithm resulted in lower construction costs than those obtained

by the application of particle swarm optimization method. Hence, the fish shoal optimization algorithm performed better than the particle swarm optimization method. It is also clear from the Tables 7.3 and 5.5 that the flow velocities in the channels are approximately the same for both the cases. Hence, fish shoal optimization performed well for the design of the minimum cost riprap riveted earthen channels.

7.6 Concluding Remarks

The fish shoal optimization has been found to be a powerful tool that can handle a variety of solution subgroups in its single computational run as against the particle swarm optimization that can involve only one type of riprap stone for the minimum cost riprap riveted earthen canal. However, particle swarm optimization would have needed three separate programs for solving three different solution models with varying penalty functions for three subgroups of riprap stones. It is also recommended to design a riveted earthen canal with inclusion of cost of land to obtain a most hydraulically efficient least cost canal.